JOURNAL OF CATALYSIS 121, 422–431 (1990)

Steady-State Kinetics of the CO–N_2O Reaction over an Alumina-Supported Rhodium Catalyst

ROBERT W. MCCABE AND CHOR WONG

Physical Chemistry Department, General Motors Research Laboratories, Warren, Michigan 48090-9055

Received April 4, 1989; revised June 13, 1989

Kinetics of the rhodium-catalyzed reaction between carbon monoxide (CO) and nitrous oxide (N_2O) were measured in a laboratory plug-flow reactor at temperatures between 550 and 700 K, space times between 0.06 and 0.26 s, and CO and N_2O partial pressures between 0.6 and 7 Torr. A brief comparison was also made between the CO–N_2O kinetics and kinetics of the CO–NO and CO–O_2 reactions. The comparison showed that the CO–N_2O reaction is an important subreaction of the CO–NO reaction (i.e., CO reacts initially with NO to produce N_2O, which undergoes further reaction with CO to yield N_2 and CO_2). The comparison also showed that the rate of the CO–N_2O reaction is much lower than rates of the CO–NO and CO–O_2 reactions (ratio of turnover frequencies at 475 K estimated as 1 (CO–N_2O) vs 7.1×10^2 (CO–NO) vs 4.4×10^5 (CO–O_2)). CO–N_2O rate measurements under differential conversion conditions at temperatures of 564 and 583 K yielded reaction orders of -1.0 ± 0.15 in CO pressure, 0.65 ± 0.1 in N_2O pressure, and -0.30 ± 0.1 in total (CO + N_2O) pressure. The reaction orders and apparent activation energy (40 ± 2 kcal/gmol) are consistent with a mechanism involving reaction between adsorbed CO and adsorbed N_2O dissociation products. The low rate of the CO–N_2O reaction compared to the CO–O_2 and CO–NO reactions suggests that, under reaction conditions characterized by high CO coverages, the rate of dissociative N_2O adsorption is slow compared to the rates of dissociative O_2 or NO adsorption.

INTRODUCTION

The principal function of rhodium in automotive exhaust catalysts is to control emissions of nitrogen oxides (*1, 2*). To this end, the reaction of nitric oxide (NO) with carbon monoxide (CO) is a major removal pathway for nitrogen oxides. Three previous studies of the NO–CO reaction over supported Rh catalysts (*3–5*) have reported the formation of N_2O as a reaction product. Cho and Shanks (*4*) have recently shown that N_2O, formed during the NO–CO reaction, undergoes further reaction with CO to produce N_2 and CO_2. The overall reaction scheme for the NO–CO reaction reported by Cho and Shanks thus involves the following three reactions:

$$CO + NO \rightarrow \tfrac{1}{2}N_2 + CO_2 \quad (1)$$

$$CO + 2NO \rightarrow N_2O + CO_2 \quad (2)$$

$$CO + N_2O \rightarrow N_2 + CO_2. \quad (3)$$

The present study provides detailed kinetics of reaction (3) over a 0.5% Rh/Al_2O_3 catalyst. As such, it is an important prerequisite to a complete understanding of that network of catalytic reactions commonly referred to as the CO–NO reaction.

EXPERIMENTAL

All experiments were carried out in a laboratory microreactor consisting of a quartz tube (6 mm i.d.) containing 100 mg of 0.5% Rh/Al_2O_3 catalyst powder between retaining plugs of quartz wool. The feed gases passed downward through a preheating zone of blank alumina prior to contacting the catalyst. The reactor tube was mounted in a tubular infrared furnace and temperatures were controlled via a feedback controller operating off of a K-type thermocouple inserted into the bottom of the catalyst bed.

The feed gases were supplied from cylinders of 1.26% N_2O in helium and either 1 or

0021-9517/90 $3.00

5% CO in helium (all gases were obtained from Scott Specialty Chemicals Co. and contained He of 99.999% purity). The N_2O was used without additional purification, but the CO was passed through a heated alumina trap to decompose metal carbonyl impurities. Mass flow controllers were used to regulate flow rates typically at a total flow rate near 150 cm^3/min. The total pressure in the reactor was maintained near atmospheric pressure; partial pressures of the reactants were varied by changing the individual flow rates while adjusting the flow rate of pure He diluent to maintain a constant total flow rate. Feed and product gases were monitored both by mass spectrometry and by gas chromatography (Porapak Q column at 323 K).

The 0.5-wt% Rh/Al_2O_3 catalyst was prepared by ion exchange of 3-mm-diameter alumina beads (145 m^2/g; 0.5 g/cm^3 apparent bulk density) with Rh hexammine from aqueous solution. The catalyst was dried, calcined in air at 775 K for 2 h, and crushed into a 50–80 mesh powder prior to use. Hydrogen chemisorption yielded an apparent fraction-exposed of 0.33 (*6*), which was used for converting mass rates to turnover frequencies (i.e., site-specific rates expressed as molecules reacted per exposed Rh atom per second). The catalyst was routinely reduced at 473 K in 5% H_2/He for 1 h prior to each day's experiments. No significant changes in activity were observed over the course of these experiments. All kinetic parameters were obtained under differential conversion conditions (N_2O conversions < 10%), in order to eliminate mass transfer and heat transfer effects. Furthermore, low reactant concentrations and high gas flow rates were employed to minimize heat transfer effects.

RESULTS

CO_2 and N_2 were the only products observed by either mass spectrometry or gas chromatography during the course of these experiments. Figure 1 shows N_2O conversion (a) and N_2O reaction rate (b) as a function of reactor space time (volume catalyst/volumetric flow rate (STP)) at 609 K. Within experimental reproducibility, conversions were linear with space time and the rate was constant, indicating both plug-flow reactor behavior and the absence of significant heat and mass transfer effects on the measured rates. The data of Fig. 1 therefore establish that kinetic parameters can be obtained directly in our reactor from experiments carried out under differential conversion conditions.

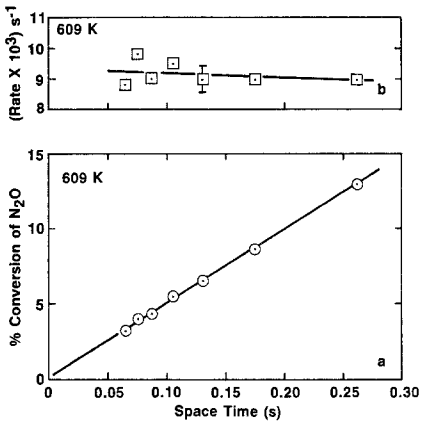

FIG. 1. Plot of conversion (a) and rate (b) for the CO–N_2O reaction as a function of space time (catalyst volume/volumetric flow rate (standard conditions)) at 609 K, 8.2 Torr CO, and 7.5 Torr N_2O.

Figure 2 shows plots of percent conversion vs temperature for stoichiometric mixtures of CO–O_2, CO–NO, and CO–N_2O. The three reactions were examined over the same catalyst sample under identical conditions. In each case, the conversion shown is that of the oxidant. The conversion of oxidant is the same as the conversion of reductant (CO) in the case of the CO–O_2 and CO–N_2O reactions, but is different in the case of the CO–NO reaction owing to different CO/NO stoichiometries for converting NO to N_2 and N_2O (see Eqs. (1) and (2) above). The dashed curve in Fig. 2 is the N_2O yield associated with the CO–NO reaction (N_2 was produced in parallel with N_2O, but is not shown in Fig. 2); N_2O yield reached a maximum near 550 K and

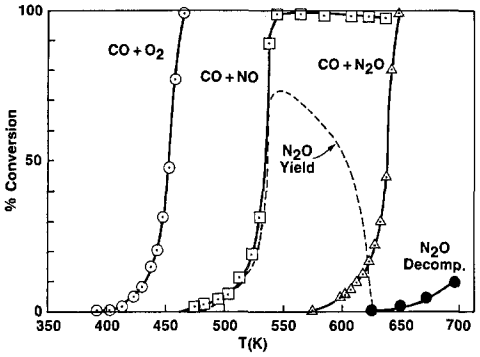

FIG. 2. Percentage conversion of oxidant species (O_2, NO, or N_2O) as a function of temperature for stoichiometric CO–O_2(1 : 0.5), CO–NO(1 : 1), and CO–N_2O(1 : 1) mixtures (150 cm³/min total flow; 4.3 Torr CO). The yield of N_2O is shown, in addition to the total NO conversion, for the CO–NO reaction. N_2O decomposition data in the absence of CO are also shown.

dropped sharply above 600 K. This sharp decrease in N_2O yield roughly correlates with the sharp increase in N_2O conversion shown for the CO–N_2O reaction above 600 K, thus lending support to the inclusion (by Cho and Shanks (*4*) of the CO–N_2O reaction as an important subreaction of the overall CO–NO reaction network. (The fall-off in N_2O yield for the CO–NO reaction in Fig. 2 begins about 25° below the onset of the CO–N_2O reaction. This can be explained in terms of different CO and N_2O partial pressures in the two cases; the CO and N_2O pressures are lower for the CO–NO reaction above 550 K than they are for the CO–N_2O reaction. We show below that decreasing the total CO + N_2O pressure increases the reaction rate and shifts the conversion vs temperature curve to lower temperatures.)

The data of Fig. 2 are of particular interest as a comparison of the relative efficiencies by which O_2, NO, and N_2O react with CO over Rh/Al_2O_3 catalyst. N_2O is especially difficult to react with CO as indicated by a 50% conversion temperature of 638 K compared to 535 K for NO and 453 K for O_2.

Large differences in rates between the three reactions are also indicated in Fig. 3, which shows Arrhenius plots of low-conversion data for each reaction. Extrapolating the curves to a common temperature of 475 K yields a ratio of turnover frequencies of 1 to 7.1 × 10^2 to 4.4 × 10^5 for the CO–N_2O, CO–NO, and CO–O_2 reactions, respectively. Fig. 3 also shows that the three reactions are characterized by markedly different apparent activation energies (31 kcal/gmol for the CO–O_2 reaction; 34.5 kcal/gmol for the CO–NO reaction; 40.5 kcal/gmol for the CO–N_2O reaction).

Despite the low rates of the CO–N_2O reaction, N_2O reacts much more rapidly in the presence of CO over Rh/Al_2O_3 than it does in the absence of CO. This is shown by the N_2O decomposition curve in Fig. 2 where temperatures near 700 K were required to obtain 10% conversion of N_2O.

The N_2O decomposition data of Fig. 2 are replotted in Fig. 4 (as curve b) along with N_2O decomposition data over blank alumina (curve a). The two curves clearly show that Rh and not the alumina support is responsible for N_2O decomposition over the Rh/Al_2O_3 catalyst. Figure 4 also shows the effects of adding a small amount of CO to the N_2O feed (curve c). At a feed ratio of 5 Torr CO to 90 Torr N_2O, the N_2O conversion reaches nearly 5% even by 575 K and then asymptotically approaches the level of 5.5% (which corresponds to complete CO

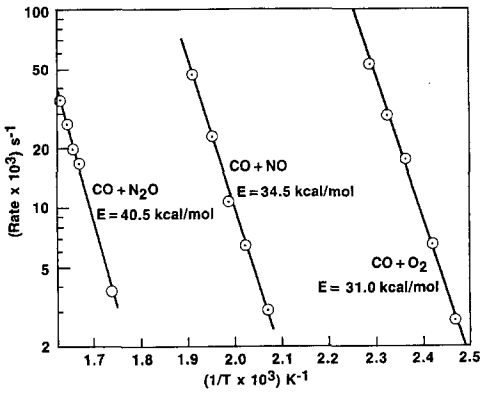

FIG. 3. Arrhenius plots for the CO–O_2, CO–NO, and CO–N_2O reactions at conditions identical to those of Fig. 2 and conversions below 10%.

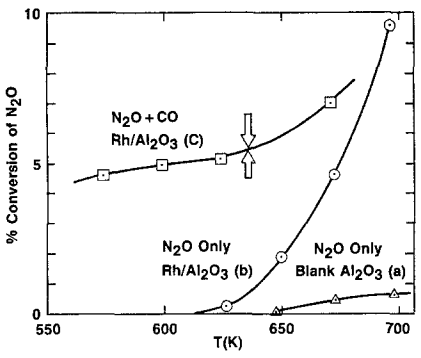

FIG. 4. Percentage conversion as a function of temperature for (a) N_2O decomposition over blank Al_2O_3, (b) N_2O decomposition over the 0.5% Rh/Al_2O_3 catalyst, and (c) the CO–N_2O reaction over the 0.5% Rh/Al_2O_3 catalyst at a feed ratio of 5 Torr CO to 90 Torr N_2O. The arrows denote the conversion corresponding to complete consumption of the feed CO.

consumption) by 625 K. Above 625 K, the conversion increases again, but only at a rate that mirrors the decomposition rate of N_2O on the Rh/Al_2O_3 catalyst (curve b). These results show that the inclusion of a small amount of CO in the feed dramatically enhances the N_2O conversion up to the point where CO is completely consumed, but has no effect beyond that point.

Although CO greatly enhanced the rate of N_2O decomposition, the extent of enhancement is greatest for small CO/N_2O ratios. This is illustrated in Fig. 5 which shows conversion vs temperature plots for two CO/N_2O feed mixtures—one with a 20% excess of CO (rich) and the other with a 20% excess of N_2O (lean). Equivalent N_2O conversions are reached at lower temperatures in the lean feed than in the rich feed. However, consistent with the lean-feed data of Fig. 4, N_2O conversion in the case of the lean feed in Fig. 5 does not extend beyond 80% where all of the feed CO is consumed.

Another illustration of lower N_2O reaction rates in rich feeds compared to those in lean feeds is given in Fig. 6 which shows plots of rate vs inverse temperature for rich and lean feeds under conditions of differential conversion. The CO–N_2O reaction rates in the 20% lean feed are greater than those in the 20% rich feed by nearly a factor of 2. The apparent activation energy is independent of feed composition, at least within the limits of reproducibility in these experiments. Values obtained in rich and lean feeds (Fig. 6) and stoichiometric feeds (Fig. 3) all fall within the range of 40 ± 2 kcal/gmol.

The lower CO–N_2O reaction rates in rich feeds result from a strong negative-order dependence of the rate on CO partial pressure. This is shown in Fig. 7 as log–log

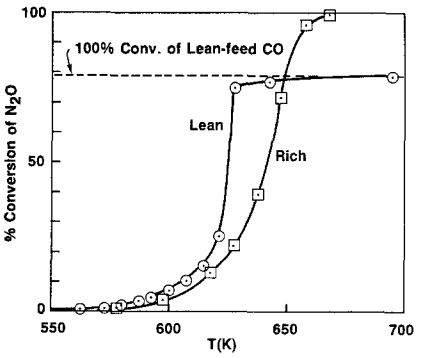

FIG. 5. Percentage conversion of N_2O as a function of temperature for feeds containing 20% excess CO (rich) and 20% excess N_2O (lean). Both the CO and N_2O pressures were changed by ±10% from the stoichiometric composition to obtain the 20% rich and 20% lean feeds.

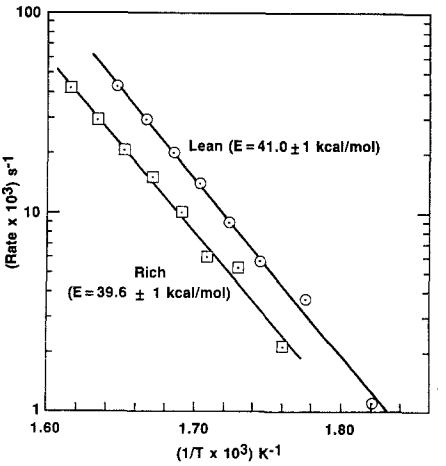

FIG. 6. Arrhenius plots at less than 10% conversion for feeds containing 20% excess N_2O (lean) and 20% excess CO (rich).

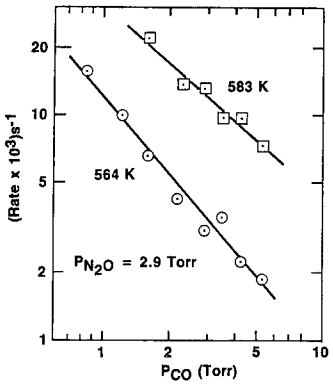

FIG. 7. Rate of the CO–N_2O reaction as a function of CO pressure at 564 and 583 K. The N_2O pressure was constant at 2.9 Torr and the total flow rate was constant at 150 cm^3/min.

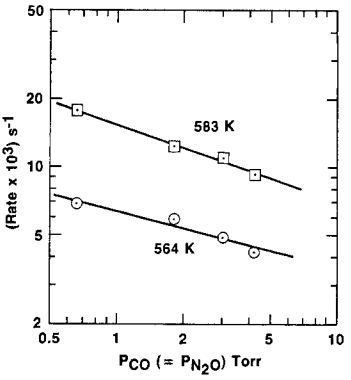

FIG. 9. Rate of the CO–N_2O reaction as a function of total CO + N_2O pressure at 564 and 583 K. CO and N_2O pressurse were equal in all cases, and the total flow rate was constant at 150 cm^3/min.

plots of rate vs CO pressure at constant N_2O pressure. Data are shown for temperatures of 564 and 583 K. The lines through the data represent linear regression analyses, yielding orders of −1.1 at 564 K and −0.86 at 583 K. Similar experiments were carried out at 564 and 583 K holding CO pressure constant and varying N_2O pressure. Results are shown in Fig. 8. Linear regression analysis yielded slopes of 0.63 at 564 K and 0.68 at 583 K.

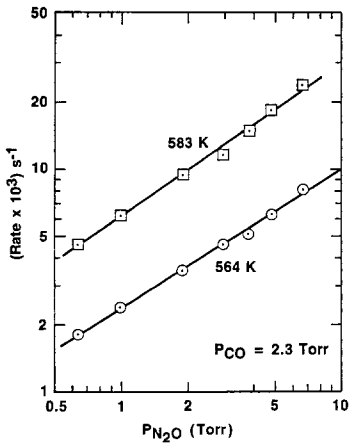

FIG. 8. Rate of the CO–N_2O reaction as a function of N_2O pressure at 564 and 583 K. The CO pressure was constant at 2.3 Torr and the total flow rate was constant at 150 cm^3/min.

Taken together, the data of Figs. 7 and 8 suggest that the total pressure dependence (CO plus N_2O partial pressures) should be negative order. This is confirmed in Fig. 9 which shows log–log plots of rate *vs* total pressure (for $P_{N_2O} = P_{CO}$) at 564 and 583 K. Reaction orders of −0.25 and −0.34 were obtained by linear regression at 564 and 583 K, respectively.

In summary, the differences in reaction orders measured at 564 and 583 K appear to be more a result of experimental variability than definite temperature-dependent trends. Overall, the kinetic data are adequately summarized as -1.0 ± 0.15 in CO pressure, 0.65 ± 0.1 in N_2O pressure, and -0.30 ± 0.1 in total (CO + NO) pressure over the range 564–583 K.

DISCUSSION

This study revealed three striking features of the CO–N_2O reaction over Rh/Al_2O_3: (1) CO greatly enhances N_2O decomposition rates, (2) the rate shows a strong negative-order dependence on CO pressure (even though CO greatly increases rates compared to N_2O decomposition rates), and (3) the rates are much lower than those of the CO–O_2 and CO–NO reactions. Each of these features is considered in turn below.

CO Enhancement of N_2O Decomposition

N_2O is generally reported to dissociate on metal surfaces by nitrogen–oxygen bond cleavage which releases N_2 directly to the gas phase and leaves a strongly chemisorbed oxygen atom behind (*7–10*). In the absence of reducing species, buildup of O-atoms on the surface rapidly poisons the decomposition reaction (*7–10*). Our data are consistent with this picture of N_2O decomposition. N_2O decomposed slowly in the pure N_2O feed (Figs. 2 and 3) at a rate characteristic of an oxidized surface. The rate was greatly accelerated by the addition of CO. However, in lean feeds, the effect of added CO did not extent beyond the point of complete CO consumption (Figs. 2 and 5). This implies that poisoning of the catalyst by O-atoms is stoichiometric; i.e., for every N_2O molecule that dissociates, a Rh surface site will be poisoned by the O-atom left behind. It should be noted that the poisoning attributed to surface oxygen is consistent with both thermal desorption experiments (*11*), which show O_2 desorbing from single-crystal Rh only at temperatures above 800 K, and supported catalyst studies showing bulk oxidation of Rh/Al_2O_3 to Rh_2O_3/Al_2O_3 at temperatures below 773 K (*6*, *12*). These studies confirm that once O-atoms are formed on a Rh surface they can only be removed through reactions with reducing species (in the temperature range of this study).

Strong CO Inhibition of the CO–N_2O Reaction

Even though CO greatly increased the rate of N_2O decomposition, the CO–N_2O reaction displayed negative first-order CO pressure dependence over the range of temperatures and partial pressures of this study. The negative first-order CO pressure dependence indicates that competitive adsorption between CO and N_2O greatly favors CO, thereby leading to high coverages of CO under reaction conditions and few available sites for N_2O adsorption. This can be shown by a first-order Langmuir competitive adsorption model for CO and N_2O using adsorption and desorption rate constants from the literature as summarized in Table 1. The Langmuir model gives

$$\theta_{CO} = \frac{K_{CO}P_{CO}}{1 + K_{N_2O}P_{N_2O} + K_{CO}P_{CO}}$$

and

$$\theta_{N_2O} = \frac{K_{N_2O}P_{N_2O}}{1 + K_{N_2O}P_{N_2O} + K_{CO}P_{CO}}. \quad (4)$$

Under typical conditions of this study (583 K, 2 Torr CO, 2.9 Torr N_2O), $K_{N_2O} = 1 \times 10^{-6}$ Torr^{-1} while $K_{CO} = 7.7$ Torr^{-1}. θ_{N_2O} and θ_{CO} are estimated as 1.8×10^{-7} and 0.94, respectively. Moreover, the calculations show that the denominator in Eq. (4) is dominated by the $K_{CO}P_{CO}$ term (over the pressure range of this study). Consequently, θ_{N_2O} varies inversely with P_{CO} and, since the reaction rate is proportional to θ_{N_2O} (see Appendix and discussion below), the rate also varies inversey with P_{CO}.

In summary, CO prevents the severe suppression of N_2O decomposition activity caused by O-atom poisoning, but it also introduces a strong inhibition of its own due to site-blocking of N_2O adsorption. The in-

TABLE 1

Kinetic Parameters for the CO–N_2O Reaction (583 K)

Parameter[a]	Source
$k_{CO}^{ads} = 1.4 \times 10^{20}$	$\sigma s_0/\sqrt{2\pi mRT_g}$ $s_0 = 0.5$ (*19*, *20*)
$k_{N_2O}^{ads} = 2.2 \times 10^{20}$	$\sigma s_0/\sqrt{2\pi mRT_g}$ $s_0 = 1$ (assumed)
$k_{CO}^{des} = 1.8 \times 10^{19}$	$1.6 \times 10^{14}\sigma \exp(-27{,}100/RT)$ (*17*)
$k_{N_2O}^{des} = 2.1 \times 10^{26}$	$1 \times 10^{13}\sigma \exp(-5000/RT)$ (*7*, *10*, *16*)[b]
$K_{CO} = 7.7$	$k_{CO}^{ads}/k_{CO}^{des}$
$K_{N_2O} = 1 \times 10^{-6}$	$k_{N_2O}^{ads}/k_{N_2O}^{des}$
$k_{diss} = 1.5 \times 10^{20}$	From data fit
$K' = 8.5$	k_{diss}/k_{CO}^{des}
$K'' = 7 \times 10^{-7}$	$k_{diss}/k_{N_2O}^{des}$

[a] Units are: molecules/cm^2 s for desorption rate constants, molecules/cm^2 s Torr for adsorption rate constants, and Torr^{-1} for the equilibrium constants K_{CO} and K_{N_2O}. K' and K'' are dimensionless. σ is the Rh surface-atom density, 1.6×10^{15} atoms/cm^2.

[b] The activation energy represents an average of values reported for Cu (*10*), Pt (*16*), and Ni (*7*) single crystals.

hibition can be lessened by going to very high N_2O/CO feed ratios (e.g., Fig. 4), but this, in turn, limits the conversion of N_2O to that associated with stoichiometric consumption of the feed CO. The inhibition can also be lessened by going to temperatures of 630 K or higher where enhanced CO desorption rates lead to lower CO coverages (e.g., at 630 K, 2 Torr CO, 2.9 Torr N_2O, we estimate $\theta_{CO} = 0.73$ by Eq. (4)). Thus, the "light-off" in the CO–N_2O conversion vs temperature profiles between 625 and 650 K in Figs. 2 and 5 corresponds to a sharp decrease in CO coverage over that temperature range.

Rate Comparison: CO–O_2, CO–NO, and CO–N_2O Reactions

As shown in Fig. 3, the CO–N_2O reaction is orders of magnitude slower than the CO–NO and CO–O_2 reactions. Mechanistic studies indicate that the surface species involved in the CO–N_2O reaction (CO, O, and possibly N and NO (*9*, *13*)) are the same as those involved in the CO–O_2 and CO–NO reactions (*15*, *16*). Since the CO–N_2O reaction involves only those surface reactions that are found in the CO–NO or CO–O_2 reactions, the sluggishness of the CO–N_2O reaction cannot be attributed to slow reactions between adsorbed species. This is apparent from Fig. 2. The fact that the CO–O_2 and CO–NO reactions both reach essentially complete conversion by 550 K establishes that reaction rates in the adsorbed layer must be rapid. In contrast, the CO–N_2O reaction shows only negligible conversion at the same temperature. Thus the overall rate of the CO–N_2O reaction does not appear to be limited by the rate of reaction between adsorbed species.

A more likely explanation for the comparatively low rate of the CO–N_2O reaction is that the rate of dissociative N_2O adsorption is lower than rates of dissociative NO and O_2 adsorption. N_2O adsorbs weakly on metal surfaces; desorption activation energies between 4 and 6 kcal/gmol have been reported for Cu (*10*), Pt (*16*), and Ni (*7*) surfaces. The weakly adsorbed N_2O serves as a percursor to dissociative adsorption (forming N_2 gas and adsorbed O-atoms) on Cu (*10*), Rh (*9*), Ni (*7*), and Ru (*8*) surfaces. The adsorbed O-atoms react with CO to form CO_2. The overall process is represented by the following set of reactions:

$$N_2O(g) + S \rightleftharpoons N_2O(a) \quad (5)$$

$$N_2O(a) \rightarrow N_2(g) + O(a) \quad (6)$$

$$CO(g) + S \rightleftharpoons CO(a) \quad (7)$$

$$CO(a) + O(a) \rightarrow CO_2(g) + 2S. \quad (8)$$

A steady-state rate expression can be derived from the set of equations above and has the form

$$r_{CO-N_2O} = k_{diss}\theta_{N_2O} = \frac{k_{diss}K_{N_2O}P_{N_2O}}{(1 + K_{CO}P_{CO})(1 + K'') - K'K_{N_2O}P_{N_2O}}. \quad (9)$$

Details of the derivation are given in the Appendix. Table 1 gives a listing of the variables and their values (as estimated from the literature). The rate constant for N_2O dissociation, k_{diss}, is the only variable that was used as a fitting constant. If we set k_{diss} at 1.5×10^{20} molecules/cm^2 s to match the measured rate of 2.7×10^{13} molecules/cm^2 s (0.017 s^{-1}) at 583 K, 2 Torr CO, and 2.9 Torr N_2O, we find that the rate expression is closely approximated by

$$r_{CO-N_2O} = \frac{k_{diss}K_{N_2O}P_{N_2O}}{K_{CO}P_{CO}}. \quad (10)$$

The calculated value of 1.5×10^{20} for k_{diss} represents a dissociation probability of 7×10^{-7} for N_2O molecules impinging at open sites on a surface largely covered by CO (i.e., the dissociation probability is given by the ratio of the dissociation rate ($k_{diss}\theta_{N_2O}$) over the sum of the dissociation and desorption rates ($k_{diss}\theta_{N_2O} + k^{des}_{N_2O}\theta_{N_2O}$), which is closely approximated by $k_{diss}/k^{des}_{N_2O} = K' = 7 \times 10^{-7}$ as shown in Table 1). Similar values of 1.4×10^{20} for k_{diss} and 7.7×10^{-7} for the dissociation probability were ob-

tained at 564 K. This compares with a dissociative sticking probability of 0.01 for O_2 employed by Oh *et al.* (*17*) in their kinetic analysis of CO oxidation on single-crystal and alumina-supported Rh catalysts.

Interestingly, Daniel *et al.* (*9*) have reported that the initial (i.e., clean surface) dissociative sticking coefficients for N_2O and O_2 on Rh(100) between 530 and 680 K are of the same order of magnitude (0.21–0.48 for N_2O vs 0.8 for O_2). Thus a major factor influencing the adsorption rates of both O_2 and N_2O during reaction with CO is a CO-induced decrease in the dissociative adsorption rate (note that this effect is present in addition to simple site-blocking by adsorbed CO; it represents the effect of neighboring CO molecules on dissociative N_2O or O_2 adsorption on *open sites* on a predominantly CO-covered surface). As noted above, the study of Oh *et al.* (*17*), as well as subsequent work by Fisher (*18*), indicates roughtly a 10^2 decrease in the dissociative O_2 sticking coefficient at high CO coverages, while the present study suggests that the corresponding decrease in the dissociative N_2O sticking coefficient is on the order of 5×10^5. This result is not unreasonable in light of the study by Daniel *et al.* (*9*) which showed strong steric effects in N_2O adsorption on Rh(100). Dissociative N_2O adsorption terminated at an O-atom coverage of 0.25 monolayer, whereas dissociative O_2 adsorption continued up to 0.5 monolayer O-atom coverage. Analogously, the present study suggests that *adsorbed carbon monoxide* plays a much stronger inhibiting role in dissociative N_2O adsorption than in dissociative O_2 adsorption. Simply put, it appears that an N_2O molecule impacting at an "open site" in a sea of CO on a Rh catalyst particle has a much smaller probability of adsorbing dissociatively than an O_2 molecule in the same situation.

Two final points regarding the kinetics of the CO–N_2O reaction are worth noting. The first is that the rate expression in Eq. (10) predicts a first-order N_2O pressure dependence rather than the observed 0.65-order dependence. In testing numerous reaction models (e.g., second-order N_2O adsorption and desorption, second-order N_2O adsorption with first-order N_2O desorption, N_2O dissociation requiring a vacant site, etc.) we were unable to develop a model that would yield a fractional-order N_2O pressure dependence while maintaining negative first-order CO pressure dependence. We speculate that the fractional-order N_2O pressure dependence reflects more complicated precursor adsorption kinetics for N_2O than the simple treatment afforded in our kinetic model.

The second point to note is that Eq. (10) predicts that the rate of the CO–N_2O reaction should have an apparent activation energy given by

$$E_{app} = E_{N_2O}^{diss} + \Delta H_{N_2O} - \Delta H_{CO}. \quad (11)$$

Noting that ΔH_{N_2O} and E_{CO}^{ads} are small, Eq. (11) can be roughly approximated by

$$E_{app} = E_{N_2O}^{diss} + E_{CO}^{des}. \quad (12)$$

E_{CO}^{des} is on the order of 27–31 kcal/gmol while data for N_2O adsorption on Cu(111) indicate that $E_{N_2O}^{diss}$ can be as high as 10 kcal/gmol (*10*). Thus the observed apparent activation energy of 50 ± 2 kcal/gmol seems consistent with a reaction mechanism where the energetics are dominated by CO desorption and N_2O dissociation.

SUMMARY

- Rates of N_2O decomposition (i.e., in the absence of CO) were negligible (<10% conversion) over the Rh/Al_2O_3 catalyst at temperatures below 700 K.
- N_2O reacted with CO over the Rh/Al_2O_3 catalyst at temperatures above 550 K to form CO_2 and N_2 as the only detectable products.
- Rates of the CO–N_2O reaction were orders of magnitude lower than rates of the CO–NO and CO–O_2 reactions under equivalent conditions. Relative turnover frequencies followed the order CO–N_2O (1); CO–NO (7.1×10^2); CO–O_2 (4.4×10^5) for stoichiometric feeds extrapolated to a common temperature of 475 K.

• The apparent activation energy for the CO–N_2O reaction was 40 ± 2 kcal/gmol.

• Under differential conversion conditions, apparent reaction orders of −1.0 ± 0.15 in CO pressure, 0.65 ± 0.1 in N_2O pressure, and −0.30 ± 0.1 in total (CO + N_2O) pressure were measured at temperatures between 564 and 583 K.

• The negative-order total-pressure dependence was manifested by a shift of the CO–N_2O "light-off" curve to lower temperatures in leaner (i.e., lower CO/N_2O) feeds.

• Simple kinetic arguments suggest that, at temperatures ≤583 K, the CO–N_2O reaction on Rh/Al_2O_3 involves a surface reaction between CO molecules and dissociated N_2O under conditions where the surface is largely covered by CO ($\theta_{CO} > 0.9$), and where the overall reaction rate is controlled by the rate of dissociative N_2O adsorption.

APPENDIX 1

Kinetic Model for the CO–N_2O Reaction

From Eqs. (6) and (8), the rate of the CO–N_2O reaction is given by

$$r_{CO-N_2O} = k_{diss}\theta_{N_2O} = k_r\theta_{CO}\theta_O. \quad \text{(A1)}$$

Steady-state balances for θ_{N_2O}, θ_{CO}, and θ_O, respectively, yield

$$k^{ads}_{N_2O}P_{N_2O}(1 - \theta_{CO}) - k^{des}_{N_2O}\theta_{N_2O} - k_{diss}\theta_{N_2O} = 0 \quad \text{(A2)}$$

$$k^{ads}_{CO}P_{CO}(1 - \theta_{CO}) - k^{des}_{CO}\theta_{CO} - k_r\theta_{CO}\theta_O = 0 \quad \text{(A3)}$$

$$k_{diss}\theta_{N_2O} - k_r\theta_{CO}\theta_O = 0, \quad \text{(A4)}$$

where we have approximated the fraction of vacant sites by $(1 - \theta_{CO})$ (in accordance with the Langmuir estimates of surface coverages noted in the text).

Equations (A2) through (A4) are readily solved by substitution to yield

$$\theta_{N_2O} = \frac{K_{N_2O}P_{N_2O}}{(1 + K_{CO}P_{CO})(1 + K'') - K'K_{N_2O}P_{N_2O}}, \quad \text{(A5)}$$

which leads, by substitution into Eq. (A1), to the rate expression given by Eq. (9) in the text. The constants K_{N_2O}, K_{CO}, K', and K'' are defined in Table 1 and in the nomenclature section below. It is clear from the parameter values in Table 1 that Eq. (9) is nearly identical in magnitude to Eq. (10).

APPENDIX 2: NOMENCLATURE

E, activation energy, kcal/gmol
ΔH, adsorption enthalpy, kcal/gmol
k, rate constant, see Table 1 for dimensions
K, equilibrium constant, $Torr^{-1}$
K', K'', ratios of rate constants (see Table 1), dimensionless
m, molecular weight, g/gmol
P, pressure, Torr
r, reaction rate, molecules/cm^2 -s or s^{-1}
R, gas constant
s_0, initial (i.e., clean surface) sticking coefficient, dimensionless
T, temperature, K

Greek Letters

σ, rhodium surface atom density, 1.6×10^{15} atoms/cm^2
θ, coverage of adsorbed species, dimensionless

Superscripts/Subscripts

ads, adsorption
app, apparent
CO, carbon monoxide
des, desorption
diss, dissociation
g, gas
N_2O, nitrous oxide
O, oxygen
r, reaction

REFERENCES

1. Taylor, K. C., *in* "Catalysis: Science and Technology" (J. R. Anderson and M. Boudart, Eds.) Vol. 5, p. 17. Springer-Verlag, Berlin, 1984.
2. Kummer, J. T., *J. Phys. Chem.* **90,** 4747 (1986).
3. Hecker, W. C., and Bell, A. T., *J. Catal.* **84,** 200 (1983); *J. Catal.* **85,** 389 (1984).
4. Cho, B. K., and Shanks, B. H., "Kinetics of NO Reduction by CO over Supported Rhodium Catalysts: Isotopic Cycling Experiments," General

Motors Research Laboratories Research Report PC-421, March 1, 1988.
5. Iizuka, T., and Lunsford, J. H., *J. Mol. Catal.* **8,** 391 (1980).
6. Wong, C., and McCabe, R. W., "Effects of High-Temperature Oxidization and Reduction on the Structure and Activity of Rh/Al_2O_3 and Rh/SiO_2 Catalysts," General Motors Research Laboratories Research Report PC-464, August 19, 1988. *J. Catal.* **119,** 47 (1989).
7. Hoffman, D. A., and Hudson, J. B., *Surf. Sci.* **180,** 77 (1987).
8. Kim, Y., Schreifels, J. A., and White, J. M., *Surf. Sci.* **114,** 349 (1982).
9. Daniel, W. M., Kim, Y., Peebles, H. C., and White, J. M., *Surf. Sci.* **111,** 189 (1981).
10. Habraken, F. H. P. M., Kieffer, E. Ph., and Bootsma, G. A., *Surf. Sci.* **83,** 45 (1979).
11. Root, T. W., and Schmidt, L. D., *Surf. Sci.* **134,** 30 (1983).
12. van't Blik, H. F. J., van Zon, J. B. A. D., Huizinga, T., Vis, J. C., Koningsberger, D. C., and Prins, R., *J. Amer. Chem. Soc.* **107,** 3139 (1985).
13. Barker, F. G., and Gasser, R. P. H., *Surf. Sci.* **39,** 136 (1973).
14. Schwartz, S. B., Schmidt, L. D., and Fisher, G. B., *J. Phys. Chem.* **90,** 6194 (1986).
15. Schwartz, S. B., Fisher, G. B., and Schmidt, L. D., *J. Phys. Chem.* **92,** 389 (1988).
16. Avery, N. R., *Surf. Sci.* **131,** 501 (1983).
17. Oh, S. H., Fisher, G. B., Carpenter, J. E., and Goodman, D. W., *J. Catal.* **100,** 360 (1986).
18. Fisher, G. B., General Motors Research Laboratories, Personal Communication, October, 1988.
19. Campbell, C. T., and White, J. M., *J. Catal.* **54,** 289 (1978).
20. Campbell, C. T., Shi, S.-K., and White, J. M., *Appl. Surf. Sci.* **2,** 382 (1979).